Supplementary Information for:

pH Jump Kinetics in Colliding Microdroplets: Accelerated Synthesis of Azamonardine from Dopamine and Resorcinol

Emily Brown,[1,2] Grazia Rovelli,[1] and Kevin R. Wilson,[1,*]

[1]*Chemical Sciences Division, Lawrence Berkeley National Laboratory, Berkeley, CA, 94720, USA*

[2]*Department of Chemistry, University of California, Berkeley, CA 94720, USA*

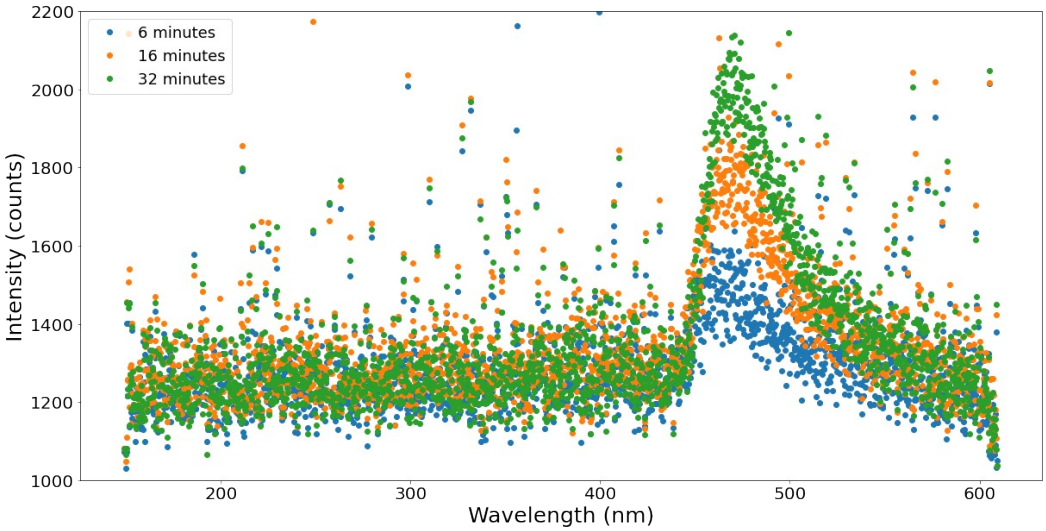

Figure S1. Dopamine (0.019 M), resorcinol (0.0047 M), NaCl (4.6 M), and carbonate-bicarbonate buffer (0.26 M, pH 9) were combined and allowed to react with constant bubbling (40 sccm air flow). Fluorescence was excited with a 355 nm laser and monitored with a spectrometer (Ocean Optics, Maya 200 pro) in order to determine if there was a second product contributing to the fluorescence signal. The only peak observed is at 475 nm, which is consistent with previous measurements and is attributable to azamonardine.[1] This suggests that the fluorescent signal measured is due solely to the formation of azamonardine.

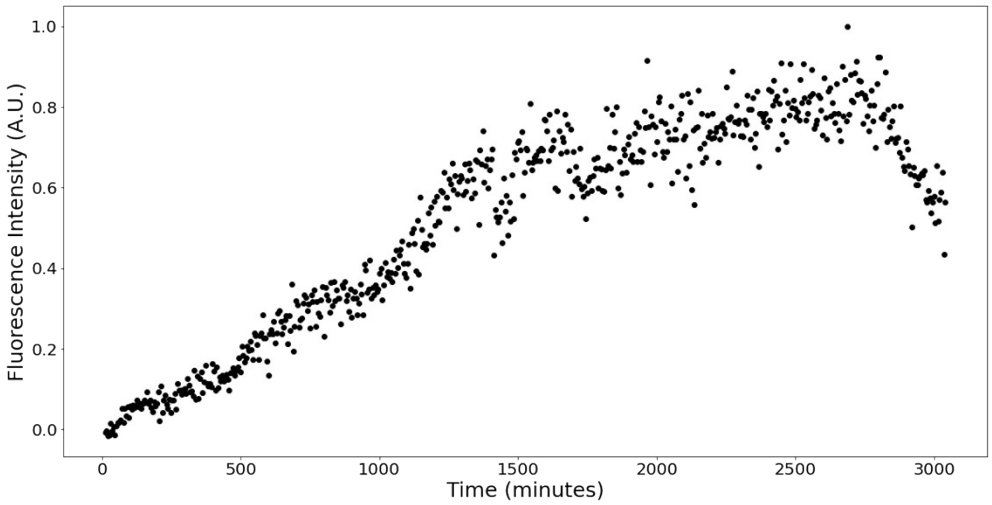

Figure S2. Fluorescence Intensity of the product azamonardine vs. time in a 20 μm radius droplet. This experiment was run with nitrogen (RH=80 +/- 3.5 %) flowing through the BQT with a flow rate of 0.3 SLM. The decrease in signal observed at 2700 minutes (i.e., ~ 2 days) is likely a result of the bleaching of azamonardine or movement of the droplet in the BQT.

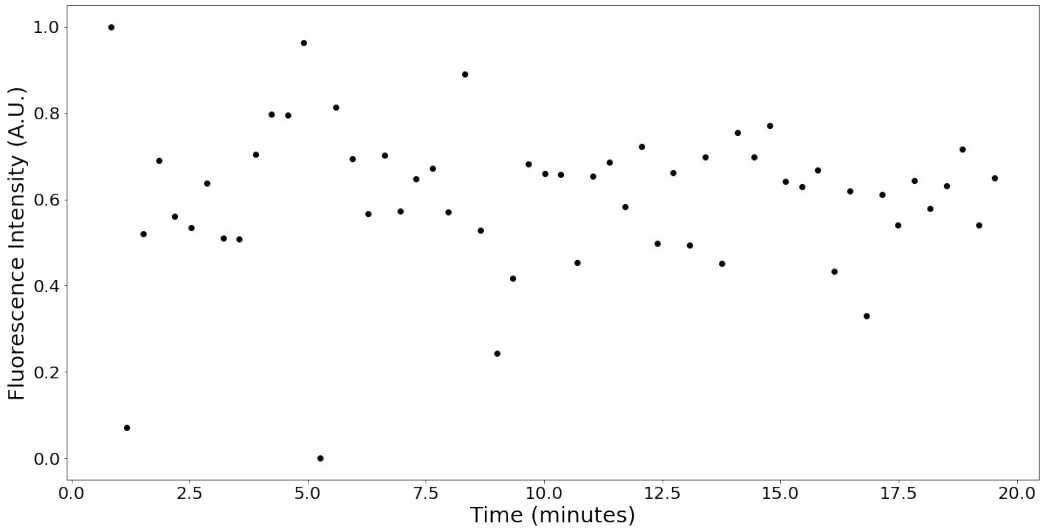

Figure S3. Fluorescence signal for a droplet (9 μm radius) with only dopamine (18 mM), resorcinol (4 mM), and NaCl (4.6 M) at pH = 5. In the absence of a buffer this reaction does not proceed.

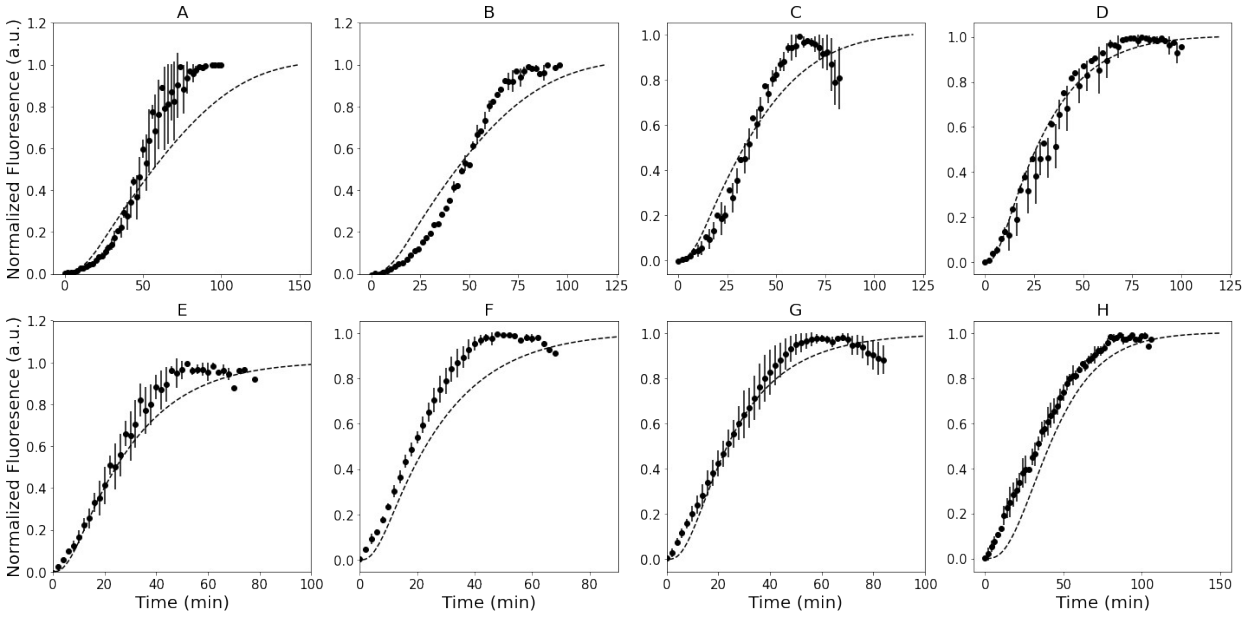

Figure S4. Experimental bulk (i.e., cuvette) kinetics and model results (dashed line) for eight concentrations of dopamine and resorcinol: 123 mM dopamine and 30 mM resorcinol (A) 83 mM dopamine and 20 mM resorcinol (B) 50 mM dopamine and 12 mM resorcinol (C) 23 mM dopamine and 6 mM resorcinol (D) 19 mM dopamine and 5 mM resorcinol (E) 12 mM dopamine and 3 mM resorcinol (F) 2.6 mM dopamine and 0.6 mM resorcinol (G) 0.2 mM dopamine and 0.05 mM resorcinol (H). The maximum fluorescence signal observed in each experiment is normalized to 1. Error bars represent 1σ uncertainty.

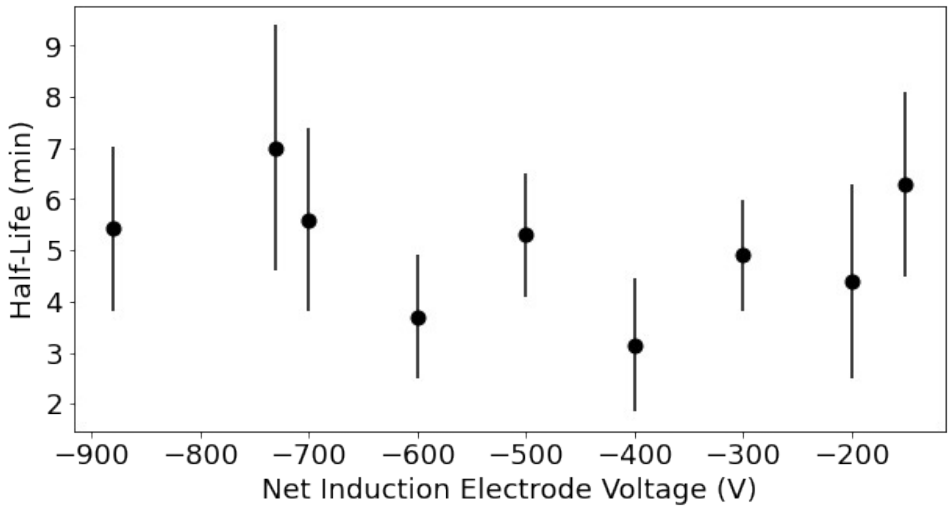

Figure S5. $\tau_{1/2}$ in droplets with an average radius of 25.3 μm as a function of net induction electrode voltage. Droplet charge scales linearly with net induction electrode voltage. A larger negative net induction electrode voltage corresponds to a stronger positive charge on the droplet. No significant trend is observed between droplet charge and product $\tau_{1/2}$. Error bars represent 1σ uncertainty.

```
{k1, k2, k3, k4, k5, kla} = {700, 420, 700, 220, 220, 30};
eqns = {
   dopa'[t] == -k1 * dopa[t] * o[t],
   dq'[t] == k1 * dopa[t] * o[t] - k2 * res[t] * dq[t],
   res'[t] == -k2 * res[t] * dq[t],
   o'[t] == -k1 * dopa[t] * o[t] - k3 * o[t] * i1[t] + kla * (0.00007 - o[t]),
   i1'[t] == k2 * dq[t] * res[t] - k3 * o[t] * i1[t],
   i2'[t] == k3 * o[t] * i1[t] - k4 * i2[t],
   i3'[t] == k4 * i2[t] - k5 * i3[t],
   aza'[t] == k5 * i3[t],
   dopa[0] == 0.12335,
   res[0] == 0.0299,
   dq[0] == 0,
   o[0] == 0.00007,
   i1[0] == 0,
   i2[0] == 0,
   i3[0] == 0,
   aza[0] == 0
  };
{dopasol, ressol, dqsol, osol, i1sol, i2sol, i3sol, psol} =
  NDSolveValue[eqns, {dopa[t], res[t], dq[t], o[t], i1[t], i2[t], i3[t], aza[t]}, {t, 0, 1000}];
```

Figure S6. Bulk kinetic model in Mathematica.

Table S1. Rate constants and other parameters used in the bulk and droplet models. Rate constants correspond to steps shown in Figure 1.

Reaction Mechanism		Rate Coefficient		
Step No.	**Elementary Step**	**Rate Constant**	**Unit**	**Ref**
1	dopamine + O_2 → DQ	1.94×10^{-20}	$cm^3\ sec^{-1}\ molecule^{-1}$	fit
2	DQ + resorcinol → 1	1.16×10^{-20}	$cm^3\ sec^{-1}\ molecule^{-1}$	[2]
3	1 + O_2 → 2	1.94×10^{-20}	$cm^3\ sec^{-1}\ molecule^{-1}$	fit [a]
4	2 → 3	3.6	sec^{-1}	[3,b]
5	3 → azamonardine	3.6	sec^{-1}	[3]
Bulk Model				
Parameter	**Equation**	**Value**	**Unit**	**Ref.**
K_LA	$\frac{d[O_2]}{dt} = K_l \cdot A \cdot ([O_2]_e - [O_2])$	0.5	sec^{-1}	fit
Droplet Model				
Parameter		**Value**	**Unit**	**Ref.**
H_{gs}		2.35	N/A	[4]
H_{sb} (4.6 M NaCl)		0.0035	N/A	[4]
Surface thickness		1×10^{-7}	cm	[5]
Dopamine diffusion coefficient		6×10^{-6}	$cm^2\ sec^{-1}$	[6]
Resorcinol diffusion coefficient		8×10^{-6}	$cm^2\ sec^{-1}$	[7]
Oxygen diffusion coefficient		1.97×10^{-5}	$cm^2\ sec^{-1}$	[8]
Maximum Surface Concentration (Γ_∞)		3×10^{14}	molecule cm^{-2}	[9]
K_{eq} Dopamine		4.21×10^{-21}	$molecule^{-1}\ cm^3$	[9]
K_{eq} Dopamine in 4.6 M NaCl		3×10^{-20}	$molecule^{-1}\ cm^3$	[c]
K_{eq} Resorcinol		1.89×10^{-21}	$molecule^{-1}\ cm^3$	[10]
K_{eq} Resorcinol in 4.6 M NaCl		3×10^{-20}	$molecule^{-1}\ cm^3$	[d]
K_{eq} DQ in 4.6 M NaCl		3×10^{-20}	$molecule^{-1}\ cm^3$	fit
K_{eq} azamonardine, **1**, **2**, **3** in 4.6 M NaCl		1×10^{-20}	$molecule^{-1}\ cm^3$	fit
$k_{desolvation}$ all organics		100	sec^{-1}	[11]

[a] k_1 and k_3 are assumed to be identical as both are the rate constants for the oxidation of similar ortho-diphenols to form quinones. Similarly, k_4 and k_5 are assumed to be equivalent. [b] The value of k_4 does not affect the model results as long as it has a value greater than ~1 min^{-1}. [c] Constrained by the literature[9,12] with specific calculations in the SI section 'Calculation of Equilibration Constants' [d] Constrained by the literature[10,12] with specific calculations and in the SI section 'Calculation of Equilibration Constants'.

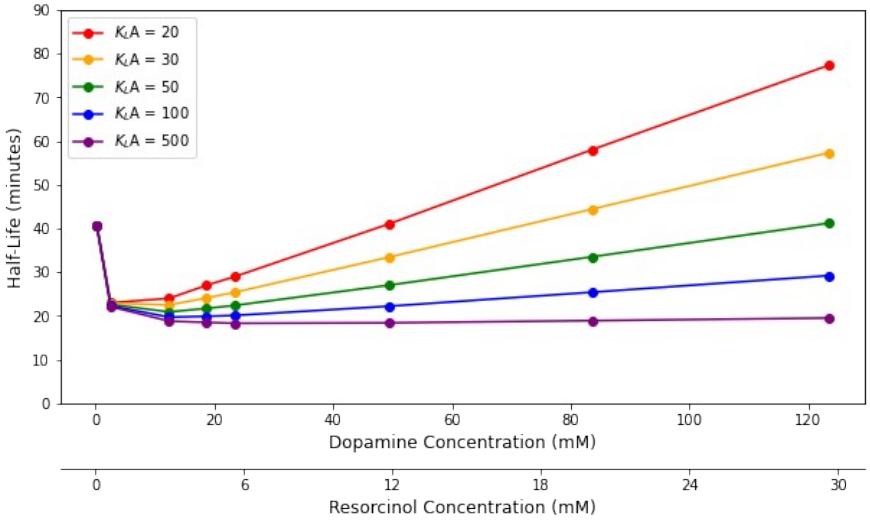

Figure S7. Bulk model results obtained by varying the K_LA (min^{-1}) and keeping all other model parameters constant. Decreasing the K_LA slows oxygen diffusion into the system and increases the $\tau_{1/2}$ for larger concentrations of dopamine and resorcinol. $\tau_{1/2}$ values at lower concentration are less impacted by the slower diffusion.

Steady State Approximation Justification

The model explicitly included oxygen adsorption and desorption to the droplet surface as well as diffusion into the bulk. A similar model using ozone has previously been published.[5] Additional model parameters required to include oxygen kinetics explicitly in the droplet model are in Table S2. From Figure S8 it is shown that the oxygen concentration reaches its expected Henry's law value even when the reaction is proceeding and that therefore the steady state approximation is justified.

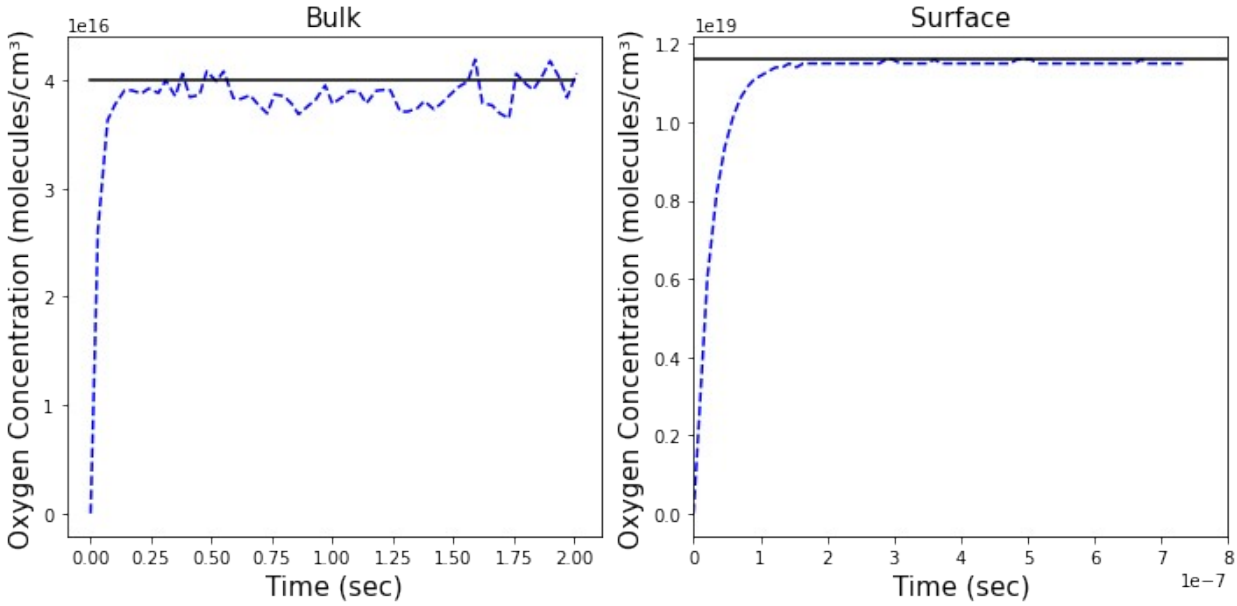

Figure S8. Simulated [O_2] in the droplet (blue) compared to the Henry's law expected concentration (black) for the bulk and surface compartments. The oxygen concentration reaches a steady state concentration before one second of reaction time in both compartments. Bulk oxygen has reached its steady state concentration within 150 ms and the surface equilibrated within 100 ns. This simulations were conducted using the kinetic framework described in Willis and Wilson using the parameters shown in Table S2.[13] The simulated droplet radius was 23 µm corresponding to a bulk compartment size of 7.67 µm.

Table S2. Additional model parameters required to model oxygen adsorption/desorption onto the droplet surface as well as solvation/desolvation into the droplet bulk compartment following the same model scheme formulated in Willis and Wilson.[5,13]

Model Parameter	Value	Unit	reference
Sticking coefficient	1	$molecule^{-1}$	[5,13,a]
Mass accommodation coefficient for oxygen	0.7	N/A	[14]
Oxygen site concentration	$5.4x10^{21}$	molecule cm^{-3}	[15,b]
Oxygen diffusion coefficient	$1.97x10^{-5}$	cm^2 sec^{-1}	[8]
k_{ads}	$7.7x10^{8}$	sec^{-1}	
k_{des}	$3.6x10^{11}$	sec^{-1}	
$k_{desolvation}$	$1.34x10^{-8}$	cm^3 sec^{-1} $molecule^{-1}$	
$k_{solvation}$	$2.52x10^{11}$	sec^{-1}	

[a] The value of the sticking coefficient had no impact on the model within the range of 1 to $1x10^{-4}$; [b] The oxygen site concentration at the surface is assumed to be identical to the ozone site concentration.

Calculation of Equilibration Constants

The maximum surface concentration (Γ_∞) is constrained to be $3x10^{14}$ molecules cm^{-2} and is consistent with prior vibrational sum frequency generation measurements of 0.5M dopamine at the air-water interface.[9] This is in close agreement with a literature value of Γ_∞ ($3.3x10^{14}$ molecules cm^{-2}) for 4-hydroxyacetophenone (4-HA), which is a similar molecule to dopamine and resorcinol in terms of both size and functional groups. The model assumes that all organic molecules compete for the same set of surface sites. The surface site concentration (Γ_∞/δ) in the simulation is $3x10^{21}$ molecules cm^{-3} using an interface thickness of δ= 1 nm.

Using Γ_∞, the equilibrium constant (K_{eq}) for partitioning of species between the bulk and the surface compartment is computed from surface tension data using the Szyszkowski-Langmuir equation[16]

$$\pi = \Gamma_\infty RTln(1 + K_{eq}x), \quad \text{(S1)}$$

where R is the gas constant, T is absolute temperature, χ is the mole fraction of the solute, and π is the surface pressure, defined as the difference in surface tension between the pure solvent and the solution. From a fit, using Eq. (S1), to the surface tension data[9] in Figure S9, K_{eq} is determined to be $4.21x10^{-21}$ cm^3 $molecule^{-1}$ for dopamine.

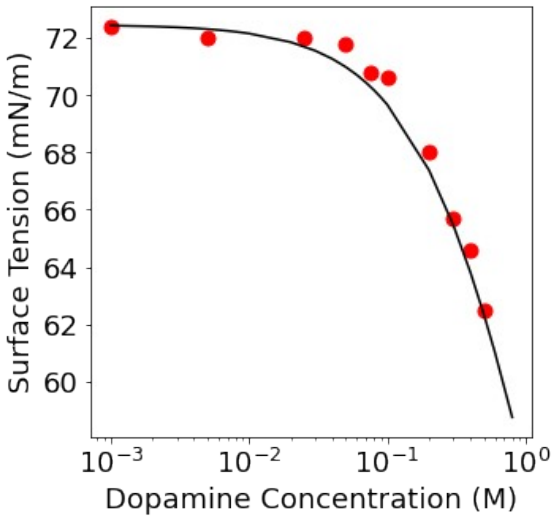

Figure S9. Surface tension vs. concentration for dopamine from Ref. [9] (red circles) plotted with a fit (black line) using Eq. (S1) with the calculated value of K_{eq} (4.21×10^{-21} cm^3 $molecule^{-1}$, and Γ_∞ constrained by the literature to a value of 3×10^{14} molecules cm^{-2}). These measurements were performed at 298 K and the surface tension of pure water found to be 72.47 mN m^{-1} .[9]

A similar procedure was followed for resorcinol, which yielded a value of 1.89×10^{-21} cm^3 $molecule^{-1}$ for K_{eq} using the same value for Γ_∞. Surface tension data for resorcinol is plotted (Fig. S10) with the fit using Eq. (S1) and this calculated value of K_{eq}.

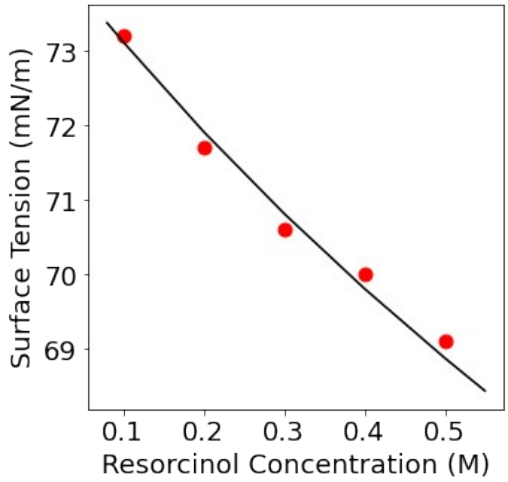

Figure S10. Surface tension vs. concentration for resorcinol from the Ref. [10] (red circles) plotted against a fit (black line) using Eq. (S1) with the calculated value of K_{eq} (1.89×10^{-21} cm^3 $molecule^{-1}$) and Γ_∞ constrained by the literature to a value of 3×10^{14} molecules cm^{-2}. The measurements were performed at 298 K, and the surface tension of pure water calibrated to 74.46 mN m^{-1}.[10]

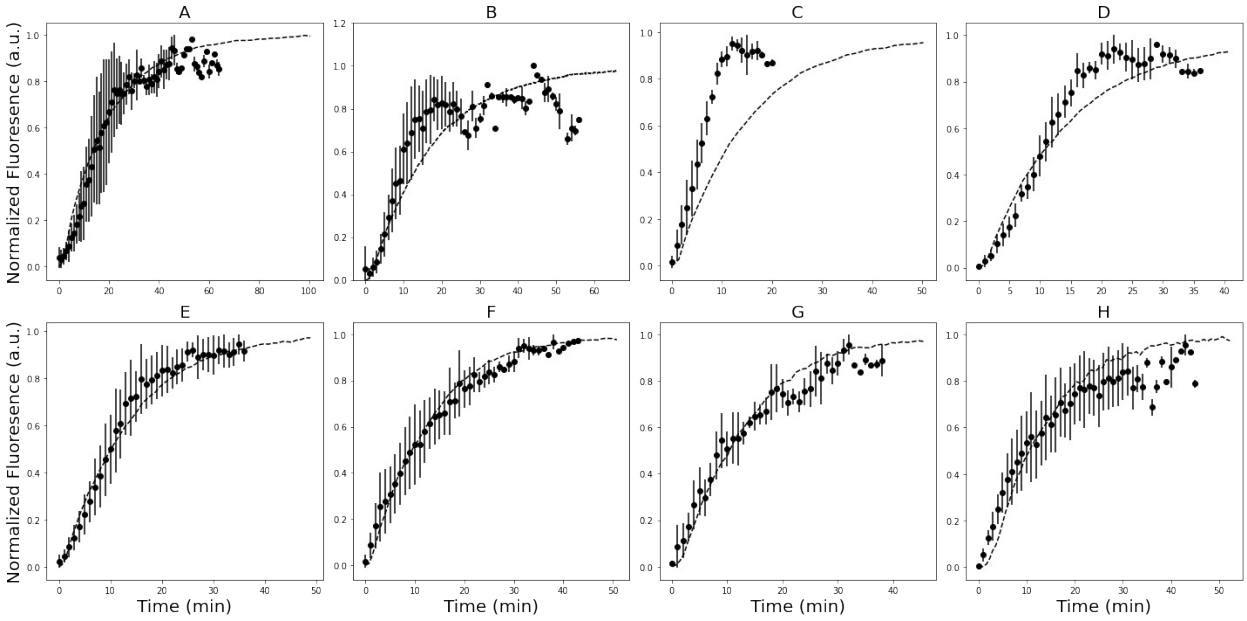

Figure S11. Experimental droplet kinetics and model results (dashed line) for eight concentrations of dopamine and resorcinol: 83 mM dopamine and 20 mM resorcinol (A) 50 mM dopamine and 12 mM resorcinol (B) 25 mM dopamine and 6 mM resorcinol (C) 19 mM dopamine and 5 mM resorcinol (D) 12 mM dopamine and 3 mM resorcinol (E) 2.6 mM dopamine and 0.6 mM resorcinol (F) 0.5 mM dopamine and 0.1 mM resorcinol (G) 0.2 mM dopamine and 0.05 mM resorcinol (H). The maximum fluorescence signal observed in each experiment is normalized to 1. The average droplet radius for all trials was 23 μm. Error bars represent 1σ uncertainty.

Table S3. Selection frequency of each step in the droplet model at the $\tau_{1/2}$ of the reaction for three different concentrations in a 23 μm radius droplet. Selection frequency is the number of times that a reaction step has been selected in Kinetiscope. As the concentrations increase a higher fraction of the steps occur in the bulk as opposed to the surface of the droplet.

Resorcinol Concentration	Dopamine Concentration		Step 1	Step 2	Step 3	Step 4	Step 5
20 mM	83 mM	Surface	6020	583	357	15	2
		Bulk	3420	2312	1097	1439	1451
		Percent occurrence at surface	**63**	**20**	**25**	**1**	**0.1**
6 mM	25 mM	Surface	7905	1375	619	24	4
		Bulk	2309	1499	834	1428	1448
		Percent occurrence at surface	**77**	**48**	**43**	**2**	**0.3**
0.053 mM	0.2 mM	Surface	2991	607	220	12	2
		Bulk	506	203	217	425	435
		Percent occurrence at surface	**86**	**75**	**50**	**3**	**0.5**

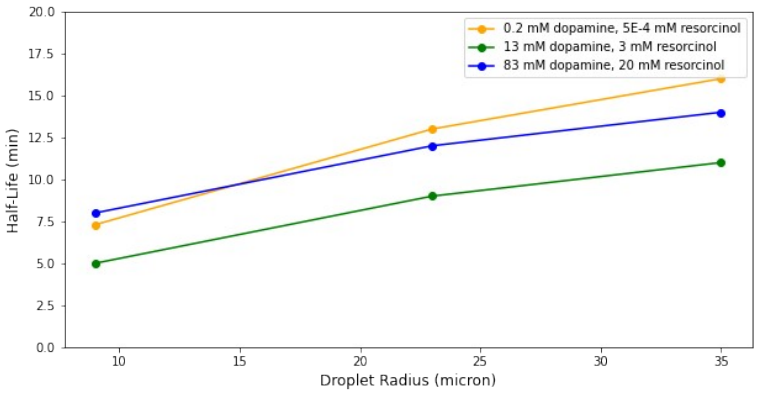

Figure S11. Droplet model results for $\tau_{1/2}$ as a function of droplet radius at three different concentrations. As dopamine and resorcinol concentrations increase the dependence on droplet size decreases as the surface becomes less important to the reaction.

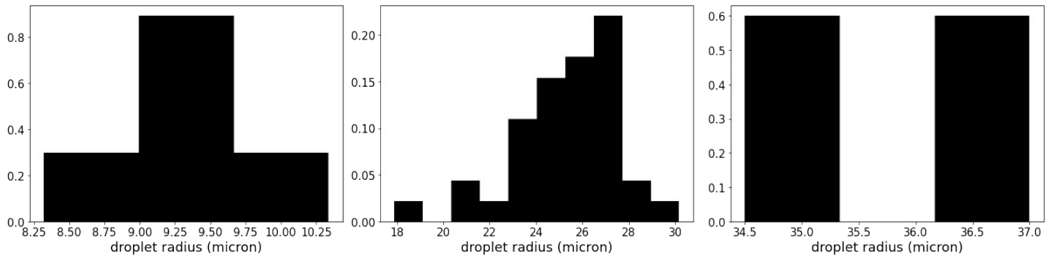

Figure S12. Histogram of final droplet radius for Figure 5 showing the spread in droplet radius.

References

(1) Zhang, X.; Zhu, Y.; Li, X.; Guo, X.; Zhang, B.; Jia, X.; Dai, B. A Simple, Fast and Low-Cost Turn-on Fluorescence Method for Dopamine Detection Using in Situ Reaction. *Anal. Chim. Acta* **2016**, *944*, 51–56. https://doi.org/10.1016/j.aca.2016.09.023.

(2) Ogata, Y.; Sawaki, Y.; Isono, M. Kinetics of the Addition of Benzenesulufinic Acid to P-Benzoquinone. *Tetrahedron* **1969**, *25* (13), 2715–2721. https://doi.org/10.1016/0040-4020(69)80013-X.

(3) Umek, N.; Geršak, B.; Vintar, N.; Šoštarič, M.; Mavri, J. Dopamine Autoxidation Is Controlled by Acidic PH. *Front. Mol. Neurosci.* **2018**, *11*. https://doi.org/10.3389/fnmol.2018.00467.

(4) Vácha, R.; Slavíček, P.; Mucha, M.; Finlayson-Pitts, B. J.; Jungwirth, P. Adsorption of Atmospherically Relevant Gases at the Air/Water Interface: Free Energy Profiles of Aqueous Solvation of N_2, O_2, O_3, OH, H_2O, HO_2, and H_2O_2. *J. Phys. Chem. A* **2004**, *108* (52), 11573–11579. https://doi.org/10.1021/jp046268k.

(5) Wilson, K. R.; Prophet, A. M.; Willis, M. D. A Kinetic Model for Predicting Trace Gas Uptake and Reaction. *J. Phys. Chem. A* **2022**, acs.jpca.2c03559. https://doi.org/10.1021/acs.jpca.2c03559.

(6) Trouillon, R.; Lin, Y.; Mellander, L. J.; Keighron, J. D.; Ewing, A. G. Evaluating the Diffusion Coefficient of Dopamine at the Cell Surface During Amperometric Detection: Disk vs Ring Microelectrodes. *Anal. Chem.* **2013**, *85* (13), 6421–6428. https://doi.org/10.1021/ac400965d.

(7) Codling, D. J.; Zheng, G.; Stait-Gardner, T.; Yang, S.; Nilsson, M.; Price, W. S. Diffusion Studies of Dihydroxybenzene Isomers in Water–Alcohol Systems. *J. Phys. Chem. B* **2013**, *117* (9), 2734–2741. https://doi.org/10.1021/jp311044a.

(8) Han, P.; Bartels, D. M. **Temperature Dependence of Oxygen Diffusion in H_2O and D_2O**. *J. Phys. Chem.* **1996**, *100* (13), 5597–5602. https://doi.org/10.1021/jp952903y.

(9) Biswas, B.; Singh, P. C. Protonation State of Dopamine Neurotransmitter at the Aqueous Interface: Vibrational Sum Frequency Generation Spectroscopy Study. *Langmuir* **2022**, acs.langmuir.1c02505. https://doi.org/10.1021/acs.langmuir.1c02505.

(10) Swearingen, L. E. Some Physical Properties of Aqueous Hydroxybenzene Solutions. *J. Phys. Chem.* **1928**, *32* (5), 785–793. https://doi.org/10.1021/j150287a010.

(11) Bleys, G.; Joos, P. Adsorption Kinetics of Bolaform Surfactants at the Air/Water Interface. *J. Phys. Chem.* **1985**, *89* (6), 1027–1032. https://doi.org/10.1021/j100252a028.

(12) Sahu, K.; McNeill, V. F.; Eisenthal, K. B. Effect of Salt on the Adsorption Affinity of an Aromatic Carbonyl Molecule to the Air−Aqueous Interface: Insight for Aqueous Environmental Interfaces. *J. Phys. Chem. C* **2010**, *114* (42), 18258–18262. https://doi.org/10.1021/jp1071742.

(13) Willis, M. D.; Wilson, K. R. Coupled Interfacial and Bulk Kinetics Govern the Timescales of Multiphase Ozonolysis Reactions. *J. Phys. Chem. A* **2022**, acs.jpca.2c03059. https://doi.org/10.1021/acs.jpca.2c03059.

(14) The Thermal Accommodation Coefficients of Gases. II. Determinations at Room and at Liquid-Oxygen Temperatures. *Proc. R. Soc. Lond. Ser. Math. Phys. Sci.* **1950**, *201* (1066), 321–329. https://doi.org/10.1098/rspa.1950.0063.

(15) Vieceli, J.; Roeselová, M.; Potter, N.; Dang, L. X.; Garrett, B. C.; Tobias, D. J. Molecular Dynamics Simulations of Atmospheric Oxidants at the Air−Water Interface: Solvation and Accommodation of OH and O_3. *J. Phys. Chem. B* **2005**, *109* (33), 15876–15892. https://doi.org/10.1021/jp051361+.

(16) Martínez-Vitela, M. A.; Gracia-Fadrique, J. The Langmuir-Gibbs Surface Equation of State. *Fluid Phase Equilibria* **2020**, *506*, 112372. https://doi.org/10.1016/j.fluid.2019.112372.